Astro2020 APC White Paper

The Occulting Ozone Observatory (O_3) Mission

Thematic Area: Planetary Systems

Principal Author:

Name: Doug Lisman
Institution: Jet Propulsion Laboratory, California Institute of Technology
Email: d.lisman@jpl.nasa.gov
Phone: 626-773-6133

Co-authors:

Edward W. Schwieterman, University of California, Riverside
Sara Seager, Massachusetts Institute of Technology
Dmitry Savransky, Cornell University
Christopher T. Reinhard, Georgia Institute of Technology
Stephanie L. Olson, University of Chicago
Timothy W. Lyons, Stephen Kane: University of California Riverside
Patrick Cote', John Hutchings: NRC-CNRC
Jason Rowe, Bishops University
Stan Metchev, University of Western Ontario
Nicholas Cowan, McGill University
Tony Hull, University of New Mexico
Sara R. Heap, University of Maryland
Margaret Turnbull, SETI Institute
Bertrand Mennesson, Jason Rhodes, Stuart B. Shaklan: Jet Propulsion Laboratory

Abstract:

The Occulting Ozone Observatory (O_3) is a small and focused starshade and space telescope mission to directly image exoplanets orbiting nearby sun-like stars. O_3 can detect exoplanets both in the habitable zone (HZ) and with more distant orbits. Detected rocky HZ planets can be characterized for atmospheric Rayleigh scattering and the potential biosignature byproduct gas ozone. A focus on ozone's prominent near-mid UV absorption feature enables the low-cost use of relatively small starshades and telescopes that operate close together for excellent retarget agility. A 16-m starshade paired with a 1-m off-axis telescope (notionally the proposed CASTOR CSA study mission) and a 20-m starshade paired with a 1.5-m on-axis telescope (notionally the proposed CETUS Probe study mission) are expected to characterize at least 1 or 2 rocky HZ planets, respectively. A preliminary implementation study indicates that both missions are likely to cost at the low end of the Decadal's medium mission range, in part because the telescopes cost is carried by another program. An O_3 dedicated 60-cm off-axis telescope gives less compelling performance and essentially adds cost in the Decadal's small mission range. O_3 can be launch ready within the next decade and would greatly inform and mitigate the risk of subsequent flagship missions.

This research was carried out at the Jet Propulsion Laboratory, California Institute of Technology, under a contract with the National Aeronautics and Space Administration.

1 Introduction

Astro 2010 recommended a decade of heavy starlight suppression technology investment. As result, the Astro 2020 committee now has before it flagship exoplanet direct imaging missions that can transform our understanding of planetary systems and may profoundly discover other habitable and perhaps inhabited worlds in our stellar neighborhood. A small starshade mission flying within the next decade will both inform and smooth the way for these flagship missions.

This paper presents a small and focused starshade and space telescope mission that targets the low end of the Decadal's medium mission cost range. Focused science objectives are a cost imperative but can still yield major breakthroughs. To image exoplanets in the habitable zone (HZ) and with more distant orbits for the first time will likely expand our understanding of planetary system diversity. To detect a potential biosignature at a rocky HZ planet would be profound. Candidate rocky planets are observed multiple times to constrain their orbit to the HZ and characterized for atmospheric Rayleigh scattering and the potential biosignature gas ozone. Ozone is a robust proxy for oxygen, likely of biologic origin, and has a prominent absorption feature in the near-mid UV. Short operating wavelengths and a modest detection SNR enable the use of relatively small starshades and telescopes to limit cost and risk and they operate close together to provide excellent retarget agility. This focused approach was first studied as the Occulting Ozone Observatory (O_3, Savransky et al 2010) and the same appropriately efficient mission name is adopted here.

This new O_3 mission operates a 16-m or 20-m starshade with a companion telescope at Earth-Sun L2 for at least 3-years with fuel for 5-years total. Three telescope options are considered to cover a range of performance and cost. Option 1 is a dedicated 60-cm off-axis telescope. Option 2 is a 1-m off-axis telescope that is *notionally* contributed by the Canadian Space Agency (CSA) as the study mission called the Cosmological Advanced Survey Telescope for Optical and UV Research (CASTOR, Cote' et al 2012), as part of a CSA-NASA mission partnership. Option 3 is a 1.5-m on-axis telescope and is notionally funded by NASA as the proposed Cosmic Evolution through UV Survey (CETUS) mission (Heap et al 2019). Other telescope options can be studied.

The remainder of this paper is organized as follows. Section 2 presents the science objectives and makes the case for targeting ozone. Section 3 gives an overview of the mission with target lists, observing strategies and budgets for ΔV and mass. Section 4 details the design and technology readiness. Section 5 presents the expected performance. Section 6 discusses preliminary implementation plans, including mission cost. Section 7 closes with a summary and conclusions.

2. Science

2.1 Science Objectives

The first science objective is to characterize planetary system diversity, including planets confirmed to be in the HZ, or in more distant orbits, and exozodiacal brightness and structure. Select planets will be observed at least four times to constrain their orbits. The second objective is to characterize candidate rocky HZ planets for the presence of an atmosphere via Rayleigh scattering and the presence of atmospheric ozone. A third objective is to identify prime target stars for future missions.

2.2 The History of Oxygen on Earth and the Case for Ozone

The most drastic chemical impact of life on Earth is the significant amount of atmospheric oxygen (O_2), currently at 21% by volume. Oxygen has long been considered a potential exoplanet biosignature given its almost exclusive production by photosynthetic life on our planet, strong chemical reactivity, and identifiable spectral signatures in the optical-NIR [Meadows et al. 2018]. Indeed, a photosynthetic biosphere that produces oxygen is also more likely to be detectable because the most basic ingredients of this metabolism (H_2O, CO_2, and photons) are likely abundant in planetary environments and allows higher productivity than possible chemosynthetic or anoxygenic biospheres (Des Marais 2000). The major spectral features of O_2 are located at wavelengths of 690 nm (O_2-B), 760 nm (O_2-A), and 1.27 μm. For similar reasons, oxygen's photochemical byproduct ozone (O_3) is also suggested as an exoplanet biosignature (Leger et al. 1993; Segura et al. 2003), producing strong absorption features at UV (200-300 nm), visible (the broad 500-700 nm Chappuis band), and mid-infrared (9.65 μm) wavelengths. Of these, the Hartley-Huggins band in the UV centered at 250 nm is by far the most sensitive to low O_2 levels, saturating at O_3 abundances of ~1 ppmv that correspond to O_2 fractions of ~1% of present atmospheric level (PAL) (Reinhard et al. 2017; Schwieterman et al. 2018).

The oxygenation history of Earth's atmosphere is multifaceted and remains under intense study (Lyons et al. 2014; Olson et al. 2018b). However, data from Earth's geochemical archive provide convincing evidence for three distinct phases with atmospheric O_2 levels near PAL for only the last 10-15% of Earth's history, as shown in Figure 1. Prior to the Great Oxidation Event (GOE) at 2.33 Ga (Luo et al. 2016), geochemical proxy data derived from sulfur mass-independent-fraction suggests $pO_2 < 10^{-5}$ PAL (Zahnle et al. 2006) and photochemical models suggest even lower O_2 values, perhaps by orders of magnitude (Claire et al. 2006; Goldblatt et al. 2009). During the Proterozoic Eon (2.5-0.54 Ga), a possible "O_2 overshoot" from the GOE gave way to pO_2 levels substantially higher than in the Archean, but far below modern. The precise abundance of pO_2 during this time is disputed, and likely varied with time. Evidence from the isotopic fractionation of Chromium isotopes suggest $pO_2 > 0.1\%$ PAL (Planavsky et al. 2018, 2014), while other estimates range up to 10-40% (Kump 2008). During the last 541 million years pO_2 levels have stabilized near modern values within a factor of ~2, concurrent with the great expansion and diversification of animal life on Earth (Reinhard et al. 2016).

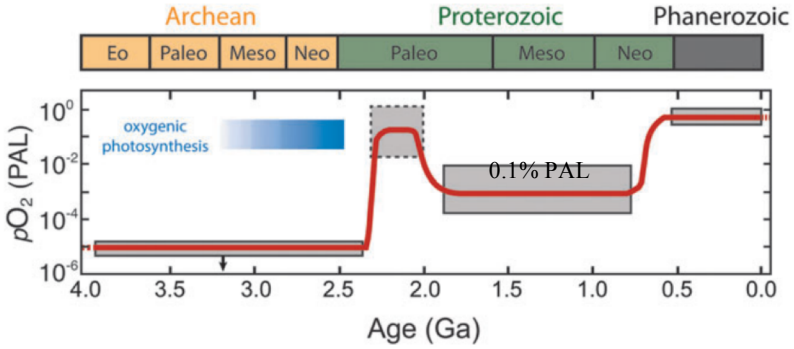

Figure 1: A schematic history of oxygen on Earth from Schwieterman et al. 2018b

If Earth's atmospheric chemical evolution provides a guide for exoplanets, then we may expect many to possess O_2 levels below O_2-A band detection limits (Reinhard et al. 2017). ***However, for***

even the lowest O_2 concentrations predicted for the Proterozoic Earth, the Hartley-Huggins ozone band would have generated a significant spectral signature (Olson et al. 2018a), making UV observations of ozone a sensitive probe to atmospheric oxygenation even at low pO_2. Figure 2a illustrates the UV O_3 band sensitivity to pO_2. At concentrations ≤ 1% PAL, decreased pO_2 results in shorter UV cutoff wavelengths until predicted O_3 abundances drop sufficiently that the band is no longer saturated at 250 nm. This shows that significant absorption occurs even at low O_2 concentrations of 10's of ppm and single-band ozone detection is less susceptible to false negatives than the O_2-A band, which shows negligible absorption low pO_2 values (see Figure 2b).

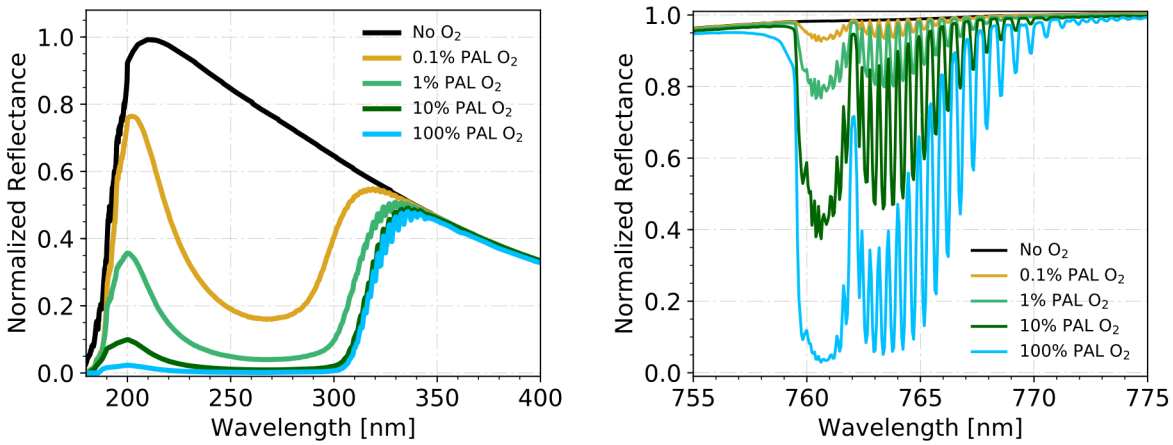

Figure 2: (a) synthetic spectra illustrating pO_2-dependent absorption by O_3 Hartley-Huggins bands, (b) absorption by the O_2-A band as a function of pO_2. The UV O_3 band is much more sensitive to low pO_2 than the O_2-A band.

Many recent papers examine the possibility of abiotic O_2 accumulation in terrestrial planet atmospheres, generating potential false positives for a photosynthetic biosphere (Meadows 2017; Harman and Domagal-Goldman 2018). Most false positive scenarios for detectable O_2 are relevant for HZ planets orbiting M dwarfs (Luger and Barnes 2015), which do not possess sufficient angular separations from their host stars to be relevant for direct imaging with small telescopes. However, some early results suggest photolysis of CO_2 and H_2O, in terrestrial exoplanet atmospheres with low H contents, may produce detectable O_3 for planets orbiting F or K dwarf stars (Domagal-Goldman et al. 2014; Harman et al. 2015). A recent study suggests that the presence of lightning, producing NO_x molecules, would effectively catalyze combinations of CO and O_2 into CO_2, negating this particular false positive scenario (Harman et al. 2018). Rarefied atmospheres lacking a tropo-spheric cold trap for H_2O may also produce abiotic O_2/O_3 through the efficient photolysis of H_2O in the stratosphere (Wordsworth & Pierrehumbert 2014). *We acknowledge that single band O_3 detection (or any molecule, including O_2) is insufficient information to claim a certain detection of life* and thus do not dwell further on false positive scenarios. However, identifying an ozone signature on a habitable zone exoplanet in the solar neighborhood would provide an extremely compelling case for follow-up observations.

In summary, the known chemical and spectral properties of atmospheric ozone, combined with our knowledge of Earth's atmospheric evolution over geologic time, suggest the intrinsic yield of detectable ozone signatures is higher than for other potential biosignature gases, like oxygen. These factors, along with the technical advantages to searching at UV wavelengths discussed below, compel us to select ozone as the target biosignature gas for the O_3 mission.

3. Mission Overview

Figure 3 shows target stars selected to provide ≥ 30% single visit HZ search completeness. O_3 will also observe a handful of known giant planets, when a detection is predicted. One observing strategy is to image all HZ targets in year-1 and then return multiple times in years 2-3 to search candidate planets for ozone and constrain their orbits. Each of the 5 60-cm HZ targets are observed twice in year-1. The search phase may be extended, based on the year-1 yield. Another strategy evaluates broadband images on the ground and a quick decision is made whether or not to stay on target to search candidate planets for ozone.

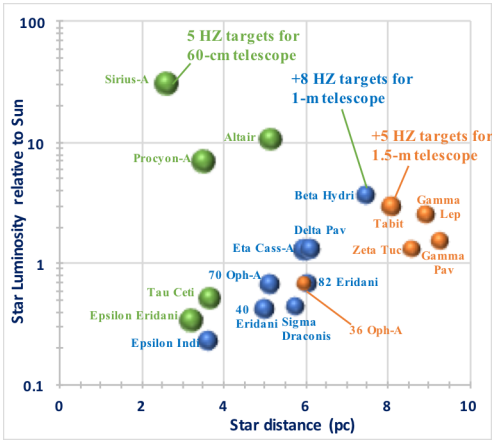

Figure 3: HZ target stars with 5, 13 and 18 stars for 60-cm, 1-m and 1.5-m telescopes, respectively.

The starshade creates an oversized dark shadow at the telescope over a 200-400 nm bandpass. A 3-band photometer instrument detects ozone from 200-300 nm, the continuum from 300-400 nm and lateral formation error from 400-500 nm. The ozone feature at the target $pO_2 \geq 0.1\%$ PAL (see figure 2A) can be identified with a relatively small SNR of 5. By comparison an ozone feature equivalent to modern Earth's can be identified with a SNR of 3.

The 60-cm telescope operates with a 16-m starshade at 16-Mm separation (S) and 172-mas inner working angle (IWA) that is well outboard of starshade tips. The 1-m telescope operates with the same starshade size and S, but gives 103-mas IWA at starshade tips. The 1.5-m telescope operates with a 20-m starshade at 30-Mm S and 69-mas IWA at starshade tips. IWAs are all set at 1.25 λ/D, where λ is 400-nm and D is aperture diameter. The reference starshade error budget provides large margins (≥ 200%, Shaklan et al 2017) for the SRM with IWA set at 1.5 λ/D and. O_3 starshades will be about 20% more sensitive to shape errors, which is well within the ample margin available.

The starshade executes retarget maneuvers with conventional biprop propulsion and carries fuel for 80 retarget maneuvers, averaging 16 per year for 5 years. An average slew-rate (dθ/dt) of 2°/day keeps star-sun angles within 40° to 83° limits for only 14 m/s of ΔV (~2Sdθ/dt) at 16-Mm S. Total retarget ΔV is thus ~1230 m/s, after adding 10% to correct navigation errors. Total ΔV is ~1930 m/s, including ΔV for formation control (210 m/s) and regular navigation at Earth-Sun L2 (100 m/s), plus 25% overall contingency. This requires ~1,000 kg of propellant.

Table 1 shows the system mass budget, for the 60-cm telescope option, with deliberately conservative estimates. There is ample 38% margin, on top of 30% dry mass contingency, for 79% of total allowable growth. This extra margin covers the 1-m telescope case, but does not cover a co-launched 1.5-m telescope case, that operates at 30-Mm S to require significantly more ΔV. In this case, the starshade launches separately and arrives on-orbit after the telescope completes its primary objectives. This helps to smooth out the combined cost profile.

Element	Mass (kg)
Starshade Payload	400
Starshade Bus System	410
Contingency dry mass at 30%	240
Propellant for 1930 m/s ΔV	1000
Jettisoned deploy control system	150
Max expect Starshade wet mass	**2200**
60-cm telescope payload	120
Photometric instrument payload	30
Telescope bus	310
Contingency dry mass at 30%	140
Propellant	30
Max expect telescope wet mass	**630**
Max expected launch wet mass	**2830**
Falcon-9 launch capacity	3900
Extra launch margin (kg)	1070
Extra launch margin (%)	**38%**

Table 1: System mass budget with large margin for 60-cm telescope

4. Design and Technology Readiness
4.1 Starshade System

The starshade is conservatively dimensioned to match current TRL5 prototypes (Willems 2018) and scale up to future missions, while providing extra shadow size for O_3's small telescopes. Figure 4 shows the 16-m starshade design that consists of an 8-m inner disk and 4-m long petals. Figure 5 shows a pathfinder petal of matching 4-m length. Figure 6 shows a 10-m disk prototype. The Deployment Control Subsystem (DCS) is shown in figure 4-left.

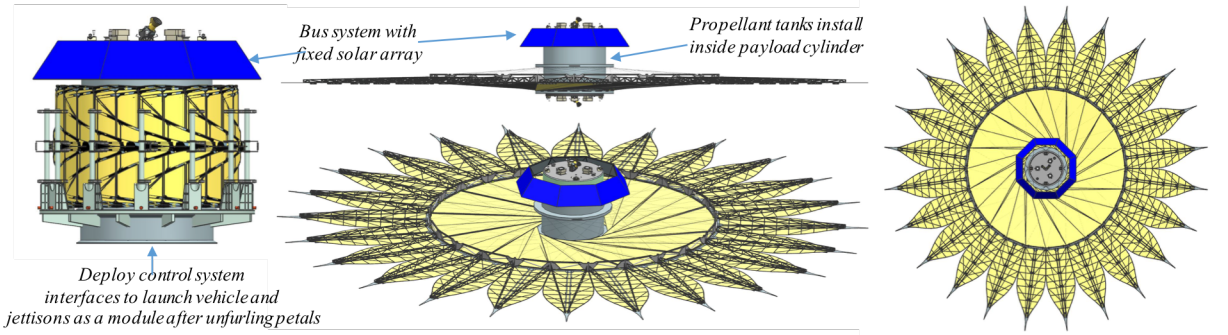

Figure 4: Starshade Configuration

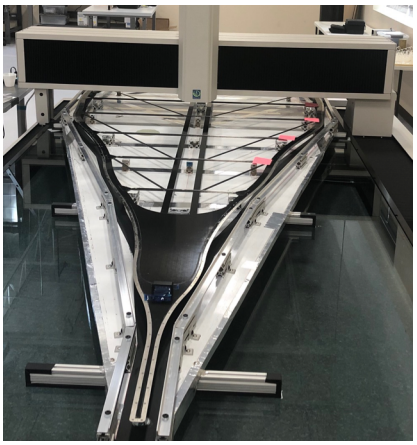

Figure 5: 4-m long pathfinder petal installed on shape metrology tool

Importantly, the petal's shape critical lateral members stow vertically and perpendicular to the petal furl direction to limit stowed strain and thus material creep. The disk's opaque optical shield stows in origami-flasher fashion to, again, limit stowed strain. The disk's perimeter truss is simplified from mesh antennae designs with bicycle-like spokes for high deployed stiffness. The DCS rotates 24 roller arms as a cassette to unfurl petals and then jettisons as a module.

The central cylinder shown in figure 6 carries bus propellant tanks and is sized to carry loads into a standard 1.6-m dia. launch-payload adapter. Bus avionics and fixed solar array install on decks at the cylinder ends. The simple Bus has low power demand, is spin-stabilized, has loose pointing requirements and no science data. Non-standard bus features are limited to a conventional, but fairly large biprop propulsion system, flight-proven Honeywell QA-3000 accelerometers to control retarget burns and S-Band transponder to communicate with the telescope and measure the separation distance. The transponder is a near copy of the direct to Earth unit, except for the exact frequency and 2-way ranging is a standard feature. All antennae are small and fixed.

Figure 6: 10-m TRL-5 disk prototype with opaque optical shield

4.2 Telescope System

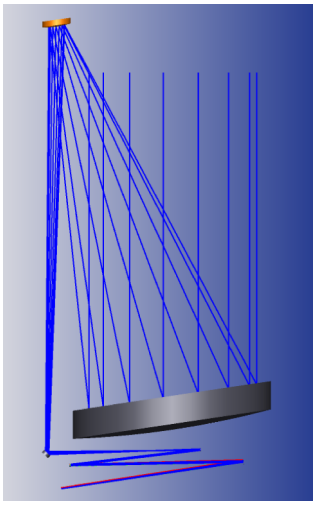

Figure 7: Optical Design

Figure 7 shows the 60-cm off-axis telescope optical design with only 6 reflections. It is diffraction limited down to 300 nm. All optics are Al coated with a MgF_2 overcoat. The Figure 8 cartoon gives more detail. The primary mirror is honeycombed thermally stable glass. The secondary mirror is actuated for post-launch alignment, but not actively controlled. The tertiary mirror is a fast-steering mirror that rejects pointing jitter. The first instrument optic stacks 2 dichroic filters and 1 flat mirror to split the beam into 3 bands. Fold and reimage mirrors place each band on a designated portion of a single 4K x 4K format conventional analog CCD, with ~3 electrons per pixel of read noise.

The continuum band (300-400 nm) pixel scale is set to Nyquist sample at 300-nm to support planet location and background object separation. Narrowband filters insert in the continuum band path to support "Rayleigh slope" detection. The ozone band (200-300 nm) is similarly sampled, but then binned on chip to read-out only 1 pixel per λ/D element, which is critical to mitigate read-noise. The formation error band (400-500 nm) senses starshade lateral position as the Poisson Spot in out of band starlight at a pupil plane and also detects tip/tilt pointing error to feed the fast steering mirror control loop.

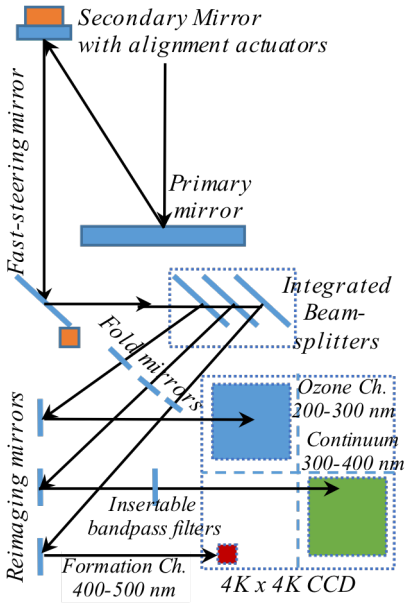

Figure 8: Optical Design Cartoon

The CASTOR baseline includes a functionally equivalent 3-channel photometer instrument of similar wavelengths and pixel scale. A small fourth channel is added at longer wavelengths for formation sensing in a pupil plane. The CETUS baseline feeds 2 spectrometers via an optical switch. Further study is required to determine if one of these spectrometers can detect ozone. Here, we assume that an O_3 dedicated photometer instrument inserts in the optical path.

The bus system for the dedicated 60-cm telescope is conventional and analogous to the WISE Explorer bus. We augment the number of reaction wheels (6 total) to mitigate a potential life limiting factor. The bus includes a small blow-down mode hydrazine propulsion system and a fixed solar array. Earth communication is via S-Band with low gain antennae for housekeeping and X-Band with fixed high gain antenna for the science data downlink, which is nominally once per week. A near-copy of the S-Band transponder, except for the exact frequency, is included for starshade communications and range measurment via 2-way ranging.

4.3 Technology Readiness

All flight equipment, except the starshade payload, is space qualified. The Starshade to TRL5 (S5, Willems 2018) activity is ongoing. The O_3 Project will advance starshade technology to TRL6-9. The Phase A/B TRL6 implementation plane is discussed further in Section 6.

5. Performance

Figure 9 shows the expected performance for each target star and telescope, in terms of planet contrast sensitivity (top), single visit rocky HZ planet search completeness (center) and expected yield of rocky HZ planets characterized after 2 visits (bottom). Key assumptions are: a median exozodi density relative to local-zodi (Z) of 4.5 (Menneson, 2019), a 20% occurrence rate, Lambertian reflectivity, a 20% geometric albedo and a mean planet radius of 1.4 R_E, that is roughly equivalent to randomly applying the size-population distribution from Fulton et al 2018. The dashed curves at the bottom of figure 9 are for 1R_E. The yield is reduced by 20% to account for a much higher Z at some stars. We conclude to expect a rocky HZ planet yield of at least 1 or 2 for the 1-m and 1.5-m telescope cases, respectively. The 60-cm telescope case may not detect any rocky HZ planets, but may be able to confirm some of the RV detected super-Earth to Neptune sized planets at Tau Ceti.

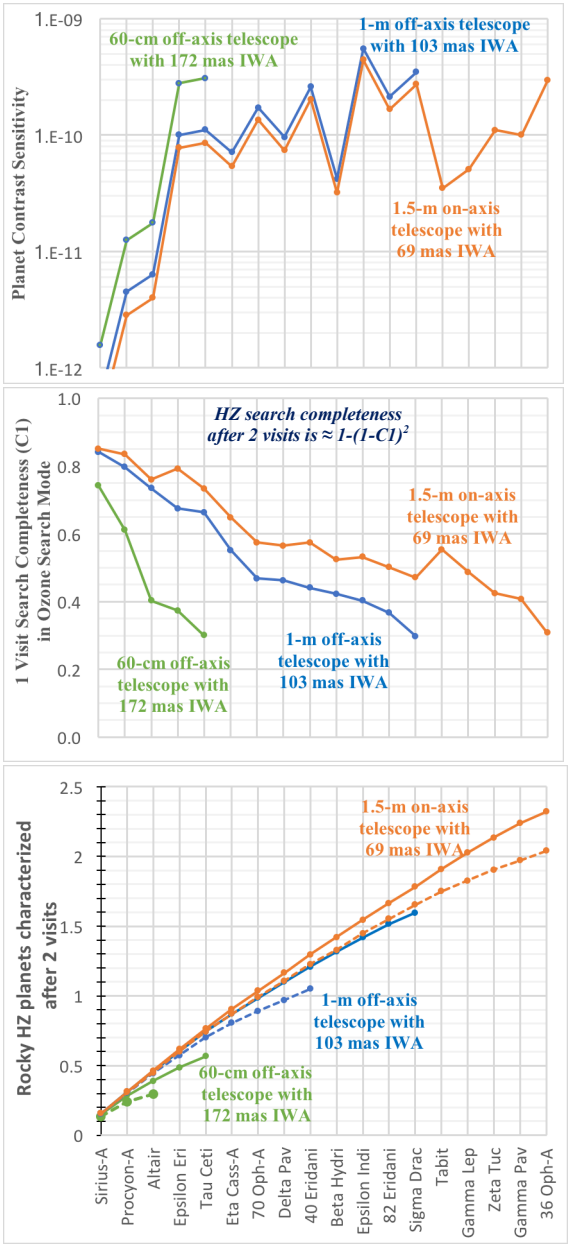

Figure 9: Planet contrast (top), search completeness (middle) & expected yield after 2 visits (bottom).

For reference, a quadrature illuminated Earth-like planet at 1AU solar equivalent distance has ~10^{-10} contrast relative to its star. The planet contrast sensitivity (C_p) shown in figure 9 is remarkably good, considering O_3's small apertures. O_3 performance is further challenged by detector read-noise that dominates required integration times. We allocate a total time on target of 30-days, but after subtracting time for read-noise, other lesser noise sources and overheads, only ~8-days remain to "integrate on exozodi". Looking at the formula used to compute C_p gives insight into how O_3 overcomes these challenges. Exozodi's contribution to integration time computes as: $t = SNR^2\ F_{ez}/F_p^2$, where F_{ez} is exozodi flux and F_p is planet flux. Planet flux is proportional to C_p. We lack space for a full derivation, but substituting equations for these fluxes and solving for C_p gives:

$$C_p = 2.14\text{x}10^{-11}\,(d^2/L)\,\sqrt{(2Z\,\frac{\lambda}{Pt})}\,(\frac{SNR}{ED^2}) = 1.64\text{x}10^{-9}\,\sqrt{(\frac{\lambda}{Pt})}\,(\frac{SNR}{ED^2})$$

where: the first constant derives from local zodi at 25 mags/arc-sec^2, 2Z accounts for exozodi looking through the full system, d is Tau Ceti distance at 3.65 parsecs, L is Tau Ceti luminosity relative to Sun at 0.52, P is the Planck function or in-band fractional energy, λ is the center-band wavelength in microns, t is time available to integrate on exozodi in seconds, D is aperture diameter in meters and $E = \varepsilon_p\,\varepsilon_{psf}\sqrt{(\varepsilon_g\,\varepsilon_o\,\varepsilon_d)}$ *is a combined efficiency factor.*

Table 2 compares individual efficiency terms for on-axis and off-axis telescope options. Table 3 compares all inputs to the above C_p formula and the resultant performance. Planet contrast sensitivity and IWA combine to constrain the detectable region within the HZ, which leads to the related HZ search completeness. The 60-cm telescope size for Option 1 was selected to give the minimally acceptable 30% HZ search completeness shown. Planet sensitivity for the 1-m telescope improves in inverse proportion to the square of aperture diameter, as expected. Planet sensitivity improvement for the 1.5-m telescope is mitigated by reduced efficiency, primarily associated with an on-axis design.

Effeciency Factors	1.5-m on-axis	60-cm or 1-m off-axis
Dynamic pointing loss, ε_p	0.9	0.9
Throughput in PSF core, ε_{psf}	0.5	0.71
Geometric Obscuration, ε_g	0.9	1
Optical throughput, ε_o	0.66	0.77
Detector quantum eff, ε_d	0.35	0.35
$E = \varepsilon_p \varepsilon_{psf} \sqrt{(\varepsilon_g \varepsilon_o \varepsilon_d)}$	**0.21**	**0.33**

Table 2: Efficiency vs. telescope

Note the strong C_p limit imposed by star distance and luminosity, per the factor d^2/L, to largely explain a limited number of target stars.

Telescope	Center-Band Wavelength λ, µm	Planck Function P	Required SNR	Exozodi time, t (days)	E	Tau Ceti planet sensitvity	IWA (mas)	HZ Search Complete-ness
60-cm off-axis	0.25	0.019	5	8.3	0.33	3.0E-10	172	30%
1-m off-axis						1.1E-10	103	67%
1.5-m on-axis				6.7	0.21	8.6E-11	69	73%

Table 3: Cp inputs and performance for Tau Ceti

The efficiency of an off-axis telescope configuration is a significant contributor to O_3 Option 1-2 performance. Other factors that all relate to ozone's prominent UV feature are:

1. Its breadth captures a reasonable fraction of the stars radiated energy, despite relatively low stellar output per unit wavelength. For example, ozone's in-band energy from Tau-Ceti almost matches the H_2O feature at 720-nm.
2. Its short wavelength offsets the limited time to integrate on exozodi.
3. Its low detection SNR partially offset small apertures.
4. Its detection via highly efficient photometer partially offset small apertures.

We also considered using a photon counting detector, to essentially eliminate read-noise, but found this to have limited benefit. The reason is that planet sensitivity is also limited by our ability to calibrate exozodi down to about the level of the planets we wish to detect. We expect to achieve ≥ 5% calibration accuracy to limit planet flux to ≥ 5% of exozodi flux. This did not come in to play for the Tau Ceti example above, but does for other target stars. Photon counting detectors will be studied further, particularly as the technology becomes more available.

6. Implementation

O_3 implementation is not yet studied in detail, but it will include heavy participation of industry and academia. JPL is the lead center and provides the optical design, optical edges, systems engineering and project management. Industry partners will provide other payload and bus systems and integrate the system. A university will provide both mission operations and science operations centers. Further study is required to fully leverage efficiencies from combining separate starshade and telescope missions. The expected Phase A-D duration is about 7 years. O_3 can be launch ready by the end of next decade, if funded to enter Phase A by FY23.

O_3 will augment S5 technology funding to accelerate the planned TRL5 completion date. O_3 advances starshade technology to TRL6 in Phase A/B per the plan detailed for the Starshade Rendezvous Probe Study (Seager et al 2019). The adopted TRL6 criterion is to demonstrate system level performance with a high-fidelity prototype. Key performance parameters, like on-orbit thermal stability, are verified by analysis with models validated via tests at subsystem or partial system levels. The smaller O_3 petals enable higher fidelity model validation. For example, we can test multiple petals together with adjoining perimeter truss bays, using available thermal vacuum chambers.

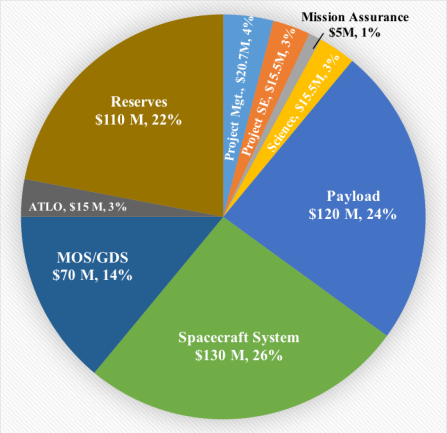

Figure 10: Cost distribution for 60-cm dedicated telescope and starshade missions.

O_3 mission cost for the dedicated 60-cm telescope option was estimated via JPL Foundry study at $500M in $FY19, including 30% reserves, but not including technology and launch services costs. Figure 10 shows the cost distribution. Flight project "wrapper costs" add about 100% to the flight element costs labeled "payload" and "spacecraft systems" that are combined here for the starshade and telescope systems.

The O_3 mission concept consists of multiple elements that were estimated using different models and methods. The objective was to provide insight as to which cost bin the project best fits in. Therefore, the project cost allocations are not estimates with high degrees of confidence but rather indicators of cost drivers based on rules of thumb for missions that may be closely analogous to O_3. Using these rules of thumb, previous Starshade mission concept studies to estimate payload costs with dollars per kilogram ratios, estimating instrument costs with the NASA instrument cost model (NICM), and CML 2 tool for spacecraft bus estimation, the project cost range was determined and clearly shows it in the Decadal's medium range. The cost uncertainty associated with this methodology is estimated by the Foundry as high as 50%.

Table 4 shows likely total mission cost ranges for all three O_3 telescope options that preserve the same wrapper cost rates shown in figure 10 and include the following augmentations:

- Falcon-9 launch services per KSC = $160M
- Starshade TRL6 campaign = $30M
- Non-mass dependent starshade costs = $20M
- Co-launched telescope cost (not 1.5-m case) = $20M
- Larger starshade cost (only 1.5-m case) = $20M

An O_3 mission with separately funded telescope likely costs at the low end of the Decadal's medium range. An O_3 mission with dedicated telescope essentially adds a second mission in the Decadal's small mission range. The cost information contained in this document is of a budgetary and planning nature and is intended for informational purposes only. *It does not constitute a commitment on the part of JPL and/or Caltech*

Cost Element	Dedicated 60-cm telescope	Separately funded 1-m or 1.5-m telescopes
Starshade Payload	60	60
Starshade TRL-6	30	30
Starshade Bus	60	60
Co-launch Tel. or larger SS	20	20
Starshade System Total	**170**	**170**
Telescope & Instrument P/L	80	0
Telescope Bus	70	0
Telescope System Total	**150**	**0**
Total Flight Development	**320**	**170**
Wrapper costs at same fig. 10 rates, with 30% reserves	320	170
Launch Cost (Falcon-9)	160	160
Likely Nominal Mission	**800**	**500**
50% Uncty (not on LV)	320	170
Likely Max Mission	**1120**	**670**

Table 4: Likely O_3 cost ranges ($M in $FY19)

7. Summary and Conclusions

This paper presents a small and focused starshade and space telescope exoplanet imaging mission called the Occulting Ozone Observatory (O_3). O_3 can detect a wide range of exoplanets in terms of size and orbital period, including rocky HZ planets, to characterize planetary system diversity and exozodiacal light. The key approach is to focus on characterizing candidate rocky HZ planets for only atmospheric Rayleigh scatter and ozone. Ozone is a robust proxy for oxygen and is likely to be of biologic origin, but a follow-on mission is required to confirm this. Ozone has a prominent absorption feature in the UV that can be detected with a relatively small telescope and starshade and a simple photometric instrument to enable this low-cost mission approach. Three telescope options are presented to cover a range of cost and performance.

Option 1 pairs a 16-m starshade with a dedicated 60-cm off-axis telescope, selected as the smallest aperture size that can still access a handful of nearby HZs, including Tau Ceti. It can serve to demonstrate the required planet sensitivity and may confirm the multiple RV detected super-Earth to Neptune size planets at Tau Ceti, but may not detect any rocky HZ planets. It is costly to fund both starshade and telescope missions and less than ideal to fly a space telescope that sits idle, while the starshade maneuvers to line up on the next target. Starshade missions are best with a separately funded companion telescope that achieves separate science objectives.

Option 2 pairs a 16-m starshade with a 1-m off-axis telescope that is notionally CSA's CASTOR study mission and requires a CSA-NASA mission partnership. This telescope improves both IWA and planet sensitivity performance to give good HZ access at 13 nearby stars and we expect *to* ***characterize at least 1 rocky planet***. Select planet orbits are constrained to the HZ with high confidence. A study is planned to more fully understand starshade accommodation by CASTOR.

Option 3 pairs a 20-m starshade with a 1.5-m on-axis telescope that is notionally the proposed CETUS Probe Class Study Mission and requires separate NASA funding. This telescope further improves both IWA and planet sensitivity to give good HZ access at 18 nearby stars and we expect *to* ***characterize at least 2 rocky planets***. Select planet orbits are constrained to the HZ with high confidence**.** A study is planned to more fully understand starshade accommodation by CETUS.

O_3 implementation is not yet studied in detail. A preliminary study suggests an Option 2-3 likely mission cost in the range of $500M to $670M, or at the low-end of the Decadal's medium mission cost range. Option 1 essentially requires funding a separate telescope mission in the Decadal's small mission cost range and is not recommended. *Note that these estimates do not represent commitments on the part of JPL and/or Caltech.*

We conclude that an early starshade mission paired with a contributed or shared telescope with aperture in the range of 1 to 1.5-m can deliver compelling exoplanet science with mission cost at the low end of the Decadal's medium mission range. Importantly, this early mission will mitigate risk and smooth the way for a subsequent flagship level mission that is required to answer our apriori questions, in addition to the new questions that this early mission is likely to raise.

References:

Bean, J. L., Abbot, D. S., & Kempton, E. M.-R. 2017, *ApJ*, 841, L24
Claire, M. W., Catling, D. C., & Zahnle, K. J. 2006, *Geobiology*, 4, 239–269
Cote', P. et al, 2012 SPIE Vol. 8442
Domagal-Goldman, S. D., Segura, A., Claire, M. W., et al. 2014, ApJ, 792, 43
Feng, F., Tuomi, M., Jones, H. R. A., et al. 2017, *AJ*, 154, 135
Fulton, B. J., Petigura, E. A., Howard, A. W., et al. 2017, AJ, 154:109
Gaudi, B. S., Seager, S., et al. 2018, The Habitable Exoplanet Observatory Mission Concept Study Interim Report
Goldblatt, C., Watson, A. J., & Lento, T. M. 2009, *Bioastronomy 2007: Molecules*, 420,
Harman, C. E., Schwieterman, E. W., Schottelkotte, J. C., et al. 2015, *ApJ*, 812, 137
Harman, C. E., Felton, R., Hu, R., et al. 2018, *ApJ*, 866, 56
Harman, C. E. & Domagal-Goldman, S. in Springer International Publishing, 2018, *Handbook of Exoplanets*, 1–22
Kasdin, N.J., et al. 2018, SPIE Vol. 10698
Kopparapu, R. K., et al. 2013, ApJ 765(2): p. 131
Kump, L. R. 2008, *Natur*, 451, 277–278
Leger, A., Pirre, M., & Marceau, F. J. 1993, *A&A*, 277, 309
Luger, R. & Barnes, R. 2015, *AsBio*, 15, 119–143
Luo, G., Ono, S., Beukes, N. J., et al. 2016, *Science Advances*, 2, e1600134–e1600134
Lyons, T. W., Reinhard, C. T., & Planavsky, N. J. 2014, *Natur*, 506, 307–15
Marais, D. 2000, *Sci*, 289, 1703–1705
Meadows, V. S. 2017, *AsBio*, 17, 1022–1052
Meadows, V. S., Reinhard, C. T., Arney, G. N., et al. 2018, *AsBio*, 18, 630–662
Mennesson, B. 2019, personal communication
Olson, S. L., Schwieterman, E. W., Reinhard, C. T., et al. 2018a, *ApJL*, 858, L14
Olson, S. L., Schwieterman, E. W., Reinhard, C. T., et al. in (Deeg, H. & Belmont, J.) Springer International Publishing, 2018b, *Handbook of Exoplanets*, 1–37
Planavsky, N. J., Cole, D. B., Isson, T. T., et al. 2018, *Emerging Topics in Life Sciences*, ETLS20170161
Planavsky, N. J., Reinhard, C. T., Wang, X., et al. 2014, *Sci*, 346, 635–638
Reinhard, C. T., Olson, S. L., Schwieterman, E. W., et al. 2017, *AsBio*, 17, 287–297
Reinhard, C. T., Planavsky, N. J., Olson, S. L., et al. 2016, *PNAS*, 113, 8933–8938
Savransky, D., Spergel, D. N., Kasdin, N. J., Cady, E. J. et al. 2010, SPIE Vol. 7731: 2H-1
Schwieterman, E., Reinhard, C., Olson, S., et al. 2018, *arXiv preprint 1801.02744*,
Seager, S. et al. 2019, Starshade Rendezvous Probe Study Report
Seager, S. et al. 2019, Whitepaper on Starshade Rendezvous Probe submitted to NAS
Segura, A., Krelove, K., Kasting, J. F., et al. 2003, *AsBio*, 3, 689–708
Shaklan, S., Marchen, L., Cady, E., 2017, SPIE Vol. 104001T
Willems, P., Starshade to TRL5 (S5) Technology Development Plan
Wordsworth, R. & Pierrehumbert, R. 2014, *ApJ*, 785, L20
Zahnle, K., Claire, M., & Catling, D. 2006, *Geobiology*, 4, 271–283